RETRAN-3D Multidimensional Kinetics Calculations for SPERT III E Tests 81 and 86

September 1999

RETRAN-3D Results for SPERT Tests 81 and 86

Introduction

Two RETRAN-3D calculations were performed to simulate SPERT experimental reactor tests[1] starting from two different conditions. These calculations were performed in response to the NRC request for additional information[2] as a demonstration of the ability of the code to simulate experimental data.

The calculations were performed with a version of RETRAN-3D MOD003 that was specially modified to read the NESTLE code[3] cross sections for the SPERT reactor. These cross sections model the unique aspects of the SPERT transient control rod. The cross-section data were supplied by the NRC as part of the request for this analysis.

RETRAN-3D Model Description

Thermal Hydraulics

The RETRAN-3D thermal-hydraulic model consists of the active core region and thermal-hydraulic boundaries. The core consists of 48 active channels and a single bypass path. Within each channel, there are 30 axial regions consisting of core thermal-hydraulic control volumes and core conductors. Figure 1 shows the thermal-hydraulic model and summaries of the model options, geometric details, and material properties are given in Tables 1 through 3. The values for thermal conductivity and specific heat for the stainless steel cladding are based upon textbook values.[4]

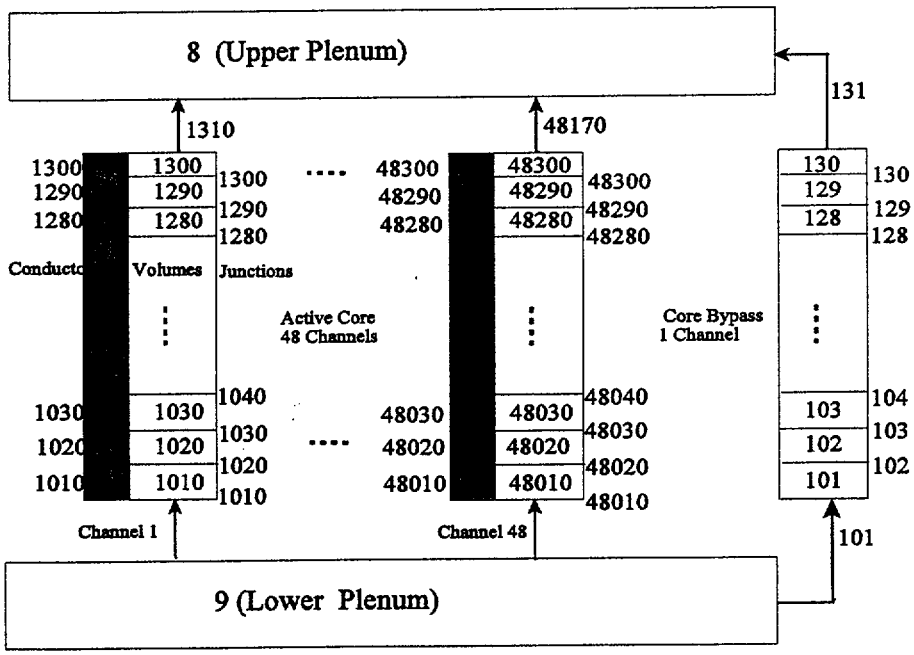

Figure 1. SPERT RETRAN-3D Model

Table 1

RETRAN-3D Model Parameters

Parameter/Model	Value	Comments
Solution Method	HEM - No Slip	No two phase conditions
Time Step Size	.5 msec	Fixed time steps
Heat Transfer Option	Default Forced Convection Map	---
Core	Full Core	---
Friction Model	Smooth Pipe	---
Enthalpy Transport	---	Core Region Only

Table 2

RETRAN-3D Flow Channel Model Parameters

Parameter	Value	Source	Comments
Flow Area (1)*	.0279 ft sq	Ref. 1	---
Flow Area (2)	.0194 ft sq	Ref. 1	---
Hydraulic Diameter (1)	.0497 ft	Based on Ref. 1 Data	4*Flow Area/Wetted Perimeter
Hydraulic Perimeter (2)	.0391 ft	Based on Ref. 1 Data	---
Heated Diameter (1)	.0497 ft	Based on Ref. 1	---
Heated Diameter (2)	.0391 ft	Based on Ref. 1	---

* (1) and (2) Refer to the two different fuel assembly configurations

Table 3

RETRAN-3D Conduction Model Parameters

Parameter	Value	Source	Comment
Fuel Rod Diameter	.42 in	Ref. 1	---
Gap Width	.003 in	Ref. 1	---
Cladding Thickness	.02 in	Ref. 1	---
Conductor Mesh Points	6	Typical RETRAN	---
Gap Mesh Points	NA	Gap Model	---
Cladding Mesh Points	2	Typical RETRAN	---
Radial Power Fraction Fuel Region	.99587	Ref. 1 - Normalized	---
Cladding Region Fraction	.00413	Ref. 1 - Normalized	---
U02 Thermal Conductivity	---	GEMP-482 Fig. 13, 86 W-cm	RETRAN PWR Sample Problem
Gap Thermal Conductivity	1000 (Btu/ft^2-hr-F)	NESTLE Input	Data File Sent With Cross Section File
Cladding Thermal Conductivity	---	Ref. 4 (Table A.6)	---
U02 Heat Capacity	---	GEMP-482	RETRAN PWR Sample Problem
Gap Heat Capacity	---	Kreith - (1 atm - .012 lbm/ft3 density)	RETRAN PWR Sample Problem
Cladding Heat Capacity	---	Ref. 4 (Table A.6)	---
Heated Length	3.197 ft	Ref. 1	---

Neutronics Modeling

A fundamental part of the kinetics response of the core is determined by the cross-section model. Typically the cross sections are generated by a physics code that can capture the state of the core in terms of historical variables such as exposure, control history, void or moderator density history, and instantaneous variables such as fuel temperature and moderator temperature. Normally, in RETRAN-3D the cross-section model data resides on an external binary file and is read according to known formats generated by three-dimensional core simulator codes.

For the SPERT calculations a cross-section file that represents the core was supplied in a format used by the NESTLE code. The details of the cross-section generation assumptions are unknown. Nevertheless, certain features regarding the structure and core layout that this file represents are known and they are discussed in the next section.

The fuel geometry data and hydraulics geometry data were derived from the SPERT III E-CORE design data in Appendix A of Reference 1. The thermal property data for core fuel material were not available from the SPERT report, therefore, the thermal conductivity and heat capacity data for the fuel pellet (UO_2) and gap was obtained from data in the RETRAN-3D PWR sample problem, and those for cladding (stainless steel) were obtained from Reference 4.

Cross Section and Core Layout

Neutronically, the SPERT core model is quite simple, consisting of three fuel assemblies types with a simple axial composition distribution. The core is an 8-by-8 fuel assembly region surrounded by a single row of cells representing the radial reflector as shown in Figure 2. There are 30 axial nodes and a single top and bottom reflector region. The cruciform transient rod moves through the center of the core, surrounded by four central fuel assemblies. There are eight assemblies that represent the remaining control rods and these are located around the core in a rotational symmetric distribution.

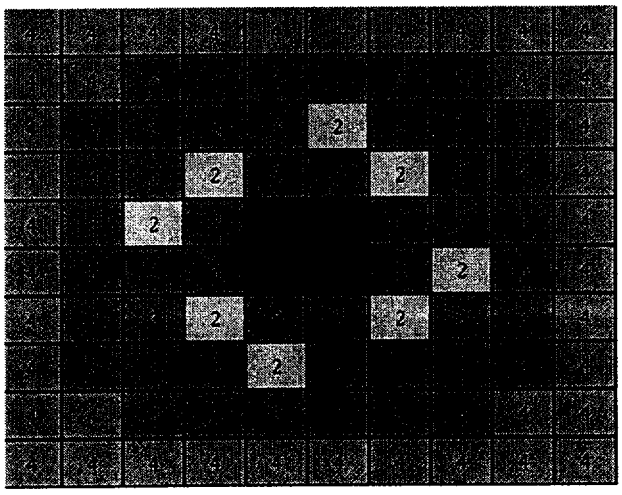

Figure 2. SPERT Core Radial Configuration

Two control rod groups are modeled to represent the physical configuration of the SPERT core. The transient rod is Group 1. The cross-section file contains sets of cross-section functions that include the effect of the transient rod insertion for the four center assemblies representing the cruciform transient rod. The control rods are collected together as a single control rod grouping as Group 2. These rods are used to achieve the initial core criticality prior to each transient.

Control Rod and Transient Rod Modeling

The modeling of the control rods in the SPERT tests is quite important to the transient results. The correct modeling of the reactivity insertion rates is required and the determination of the correct ejected rod worth is of primary importance.

In preparation for the higher power excursions, the SPERT core control rods were withdrawn to a predetermined position, and then the reactor was maintained at critical by inserting the poison section of the transient rod into the lower part of the core. The excursions were initiated by ejecting the transient rod poison section from the bottom of the core.

This process was modeled in RETRAN-3D by first positioning the transient rod to the 15.24 cm position in the core (at the top of the lower reflector). Then a criticality search was performed manually by moving the control rod positions until a critical condition was obtained by observing the steady-state eigenvalue at initial state of the core.

For Tests 81 and 86, the ejected rod worth was $1.17. The rod worth was modeled in RETRAN-3D by moving the transient rod with the thermal-hydraulic feedback frozen at the initial conditions until the desired rod worth was obtained.

The initial steady-state condition was obtained by inserting the transient rod to the predetermined position that gave the desired rod worth, then withdrawing the control rods until reactor criticality was achieved. The power excursion was modeled by dropping the transient control rod until the poison section was out of the bottom of the core. The rate at which the transient rod was dropped was determined by the design acceleration of 2000in/sec^2. The initial conditions are reported for the individual tests in the next section.

Results

Test 81

SPERT Test Number 81 is one of the low initial power test cases. The steady-state core power is 0.9MW which represents the hot-standby condition. The amount of reactivity insertion is $1.17. Other test conditions are summarized in Table 4.

Table 4

SPERT Test 81

Total Power	0.9 MW
Transient Rod Design Acceleration	2000 in/sec2
System Pressure	1500 psia
Coolant Flow Rate	1322.78 lbm/sec ft^2
Coolant Inlet Temperature	500° F
Ejected Rod Worth	1.17$

Initial Control Rod Positions (cm above bottom of core)

Rod Group	Position
1	38.86 cm
2	89.02 cm

RETRAN-3D results for Test Number 81 are shown in Figures 3 and 4, with comparisons to experimental data for transient power, and released energy. The experimental data were obtained from Reference 1, Appendix D, Figure D-65.

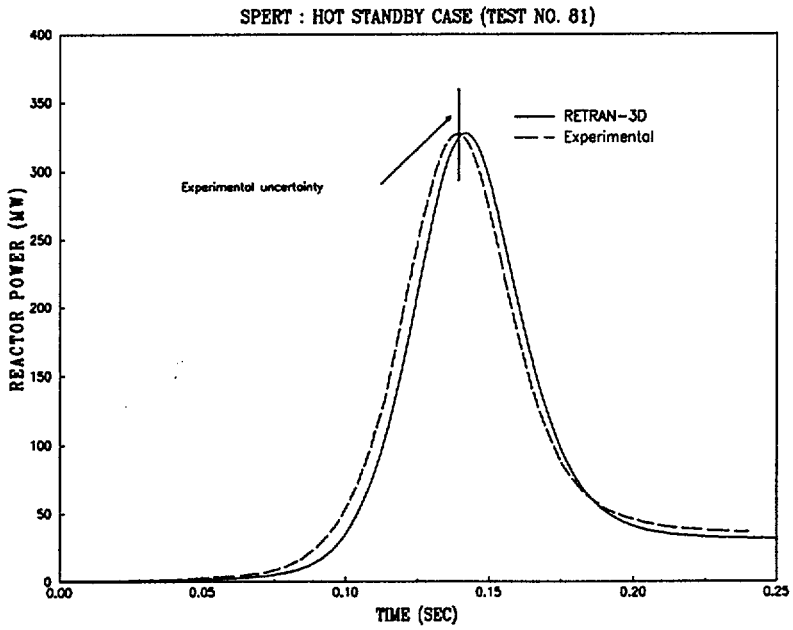

Figure 3. SPERT: Hot Standby Case (Test No. 81) - Reactor Power

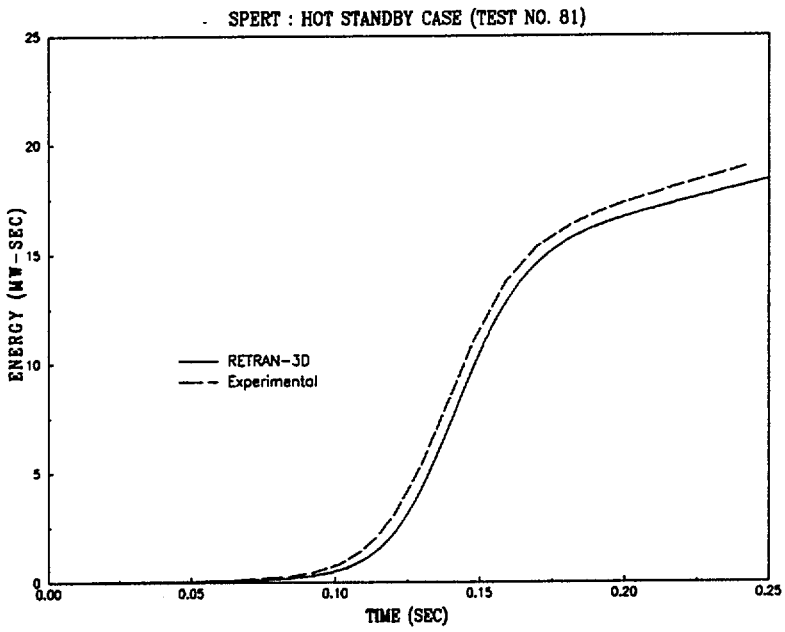

Figure 4. SPERT: Hot Standby Case (Test No. 81) - Energy

The plots show good agreement between the RETRAN-3D results and the experimental data. RETRAN-3D captured both the time and the magnitude of the peak power. There is a small difference between RETRAN-3D and the reported power after the excursion.

Test 86

SPERT Test Number 86 is a full power test case. The initial core power is 19 MW, the amount of reactivity insertion is $1.17. Some of the more relevant test conditions are summarized in Table 5. The source for the cross sections and reactivity modeling were identical to that described for Test 81.

Table 5

SPERT Test 86 Conditions

Total Power	19 MW
Transient Rod Design Acceleration	2000 in/sec2
System Pressure	1500 psia
Coolant Flow Rate	1322.78 lbm/sec ft^2
Coolant Inlet Temperature	500° F
Ejected Rod Worth	1.17$

Initial Control Rod Positions (cm above bottom of core)

Rod Group	Position
1	35.03 cm
2	79.72 cm

RETRAN-3D results for Test Number 86 are shown in Figures 5 and 6 which illustrate comparisons for transient power and released energy. The experimental data were obtained from Reference 1, Appendix D, Figure D-70.

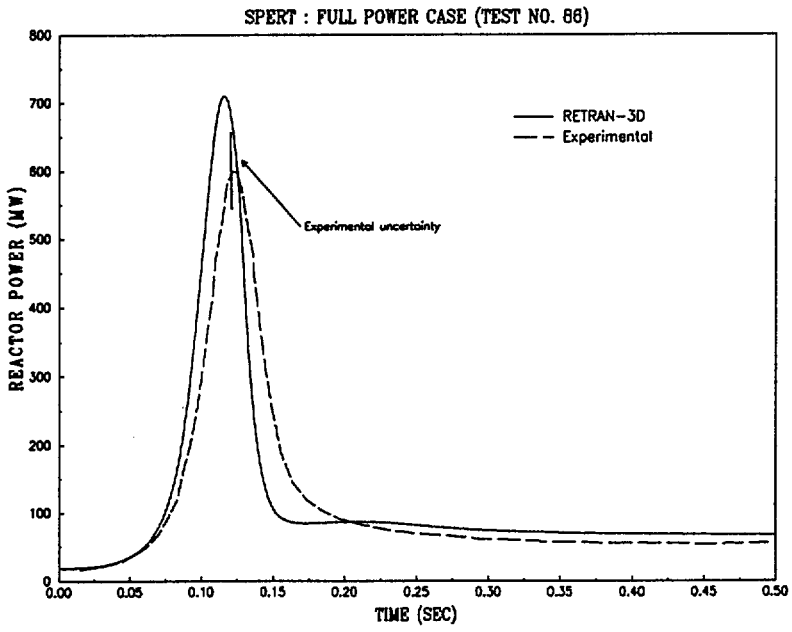

Figure 5. SPERT: Full Power Case (Test No. 86) - Reactor Power

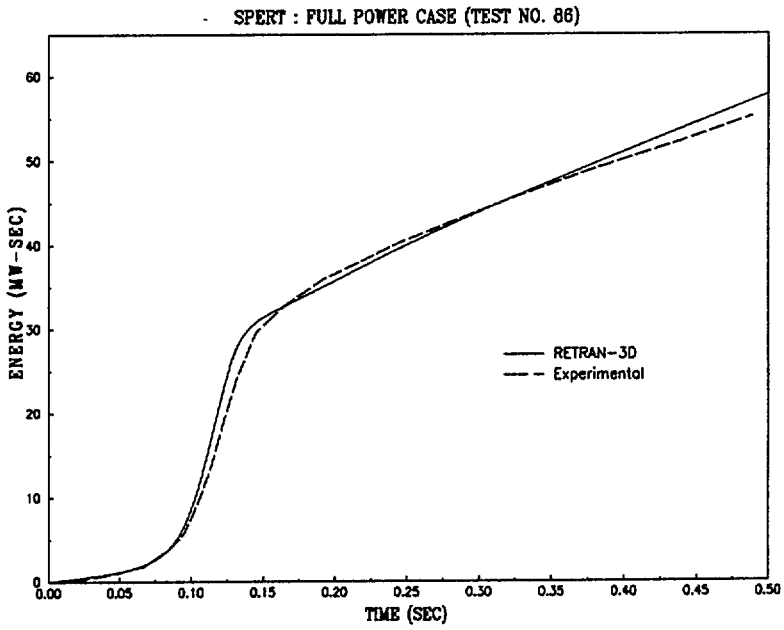

Figure 6. SPERT: Full Power Case (Test No. 86) - Energy

In general, the results are similar to those obtained in Test 81, but the magnitude of the calculated power peak is higher than that reported. It is noted here that the experimental power peak reported in Reference 1, p. 53, Table VII was 610 MW at 0.110 sec. The experimental power peak plotted in Figure 4, however, was 598 MW at 0.122 sec (Appendix D Figure D-70).

Conclusions

RETRAN-3D results have been presented for SPERT Tests 81 and 86. They indicate that many of the fundamental trends in both tests are correctly simulated. The timing and the magnitude of the peak power is predicted in both cases, suggesting that the transient reactivity insertion rate and the Doppler feedback mechanisms are reasonably modeled.

Acknowledgment

The cross section data for this analysis were supplied by Dr. Tony Ulses of the USNRC. The generation of cross sections for a specific test can involve a significant analysis effort and the authors of this report gratefully acknowledge his work.

References

1. "Reactivity Accident Test Results and Analyses for the SPERT III E-CORE, A Small Oxide Fueled, Pressurized-Water Reactor", IDO-17281, March 1969.

2. Letter from S. Dembek to G. B. Swindlehurst,, "Request for Additional Information, EPRI Topical Report 7450, RETRAN-3D", August 25, 1999, Project No. 669.

3. Al-Chalabi, Rifat M., et al., "NESTLE: A Nodal Kinetics Code", Transactions of the ANS, Vol. 68, June 1993.

4. Nuclear Reactor Engineering, Glasstone and Sesonske, 3rd Edition, Van Nostrand Reinhold, 1981.

Attachment 4
A Scalar Macroscopic Momentum Balance for Multidimensional Fluid Flow

A Scalar Macroscopic Momentum Balance for Multi-dimensional Fluid Flow

T. A. Porsching

October 15, 1999

1 Notation

Ω: Three dimensional control volume
V_Ω: Volume of Ω
$\partial\Omega$: Boundary of Ω
$S_i,\ i = 0, 1, 2$: Cross sections of Ω
A_i: Area of S_i
L_0: Length of Ω with respect to S_0
W_i: Mass flow rate through S_i
$\mathbf{n}_i$: Unit normal vectors to S_i
$W_{i,0},\ i = 1, 2$: Mixed mass flow rate through S_i
$\theta_i,\ i = 1, 2$: Angle between $\mathbf{q}_i$ and $\mathbf{n}_i$
$\theta_{i,0},\ i = 1, 2$: Angle between $\mathbf{q}_i$ and $\mathbf{n}_0$ or between $\mathbf{n}_i$ and $\mathbf{n}_0$
$\partial\Omega_i,\ i = 1, 2$: Portions of $\partial\Omega$ lying on either side of S_0
$\mathbf{N}$: Unit exterior normal vector to $\partial\Omega$
$\mathbf{q}$: Fluid velocity vector
ρ: Fluid density
p: Fluid pressure
∇: Gradient operator
$\mathbf{f}$: Body force vector

2 A Scalar Momentum Model

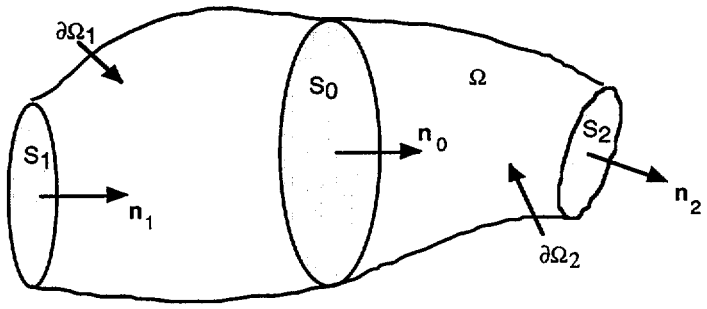

Consider the (macroscopic) control volume Ω shown in the above figure. We assign unit normal vectors $\mathbf{n}_i$ to the (planar) cross sections S_i, $i = 0, 1, 2$. Note that S_1 and S_2 are part of $\partial\Omega$, the boundary of Ω, whereas S_0 is in the interior of Ω. That part of $\partial\Omega$ not corresponding to S_1 or S_2 is assumed to be a rigid no-slip wall.

To obtain a scalar form of the momentum balance we start with the multi-dimensional Euler equations written in vector form as

$$(\rho\mathbf{q})_t + \nabla\cdot(\rho\mathbf{q}\mathbf{q}^T) + \nabla p = \mathbf{f}, \tag{1}$$

where $\mathbf{q}\mathbf{q}^T$ is a dyadic product. We take the dot product of (1) with $\mathbf{n}_0$ and integrate the result over Ω to get

$$\int_\Omega (\rho\mathbf{q}\cdot\mathbf{n}_0)_t\,dV + \int_\Omega \nabla\cdot[\rho\mathbf{q}(\mathbf{q}\cdot\mathbf{n}_0)]\,dV + \int_\Omega \nabla\cdot(p\mathbf{n}_0)\,dV = \int_\Omega \mathbf{f}\cdot\mathbf{n}_0\,dV. \tag{2}$$

Since $\mathbf{n}_0$ is a constant vector, the operations of differentiation and projection (i.e., "dotting") can be interchanged. Thus equation (2) is exact but, unlike the *vector* equation (1), it is a *scalar* equation. Let us denote the four terms of (2) respectively by I_i, $i = 1, \ldots, 4$. We treat these as follows.

$$I_1 \equiv \int_\Omega (\rho\mathbf{q}\cdot\mathbf{n}_0)_t\,dV = \frac{d}{dt}[(\rho\mathbf{q})_0\cdot\mathbf{n}_0]V_\Omega, \tag{3}$$

where the equality follows from the Mean Value Theorem for integrals and $(\rho\mathbf{q})_0$ means that the quantity $\rho\mathbf{q}$ is to be evaluated at an appropriate point in Ω as demanded by the Theorem.

If we define the mass flow rate

$$W_i = (\rho \mathbf{q})_i \cdot \mathbf{n}_i A_i,$$

then we can write (3) in the form

$$I_1 = L_0 \frac{dW_0}{dt}, \tag{4}$$

where $L_0 \equiv V_\Omega / A_0$ can be interpreted as the "length" of Ω with respect to the cross section S_0.

Next we have

$$\begin{aligned} I_2 \equiv \int_\Omega \nabla \cdot [\rho \mathbf{q}(\mathbf{q} \cdot \mathbf{n}_0)]\, dV &= \int_{\partial\Omega} (\rho \mathbf{q} \cdot \mathbf{N})(\mathbf{q} \cdot \mathbf{n}_0)\, dS \\ &= \pm \int_{S_2} (\rho \mathbf{q} \cdot \mathbf{n}_2)(\mathbf{q} \cdot \mathbf{n}_0)\, dS \pm \int_{S_1} (\rho \mathbf{q} \cdot \mathbf{n}_1)(\mathbf{q} \cdot \mathbf{n}_0)\, dS \\ &= \pm W_2(\mathbf{q}_2 \cdot \mathbf{n}_0) \pm W_1(\mathbf{q}_1 \cdot \mathbf{n}_0). \end{aligned} \tag{5}$$

In (5) the first equality follows from the Divergence Theorem while the second results from the fact that $\mathbf{q}|_{\partial\Omega} = \mathbf{0}$ except possibly on S_1 or S_2 and on S_i, $\mathbf{N} = \pm \mathbf{n}_i$, the + or − sign holding as $\mathbf{n}_i$ is an exterior unit normal or not. The third equality is again a consequence of the Mean Value Theorem for integrals.

Defining the "mixed" mass flow rate

$$W_{i,0} = (\rho \mathbf{q})_i \cdot \mathbf{n}_0 A_i,$$

we see that (5) can be written as

$$I_2 = \pm \frac{W_2 W_{2,0}}{A_2 \rho_2} \pm \frac{W_1 W_{1,0}}{A_1 \rho_1}. \tag{6}$$

For the pressure term we have

$$\begin{aligned} I_3 = \int_\Omega \nabla \cdot (p \mathbf{n}_0)\, dV &= \int_{\partial\Omega} p \mathbf{n}_0 \cdot \mathbf{N}\, dS \\ &= \pm p_1 \int_{\partial\Omega_1} |\mathbf{n}_0 \cdot \mathbf{N}|\, dS \pm p_2 \int_{\partial\Omega_2} |\mathbf{n}_0 \cdot \mathbf{N}|\, dS, \end{aligned} \tag{7}$$

where the + or − sign is chosen as $\partial\Omega_i$ is on the same side of S_0 as $\mathbf{n}_0$ or not. In (7) we have made use of the Divergence Theorem, the Mean Value Theorem for integrals, and the fact that $\partial\Omega = \partial\Omega_1 \cup \partial\Omega_2$.

Relative to a local Cartesian coordinate system whose origin is in S_0 and whose positive z-axis is directed along $\mathbf{n}_0$ we assume that $\partial\Omega_i$ can be represented by an equation of the

form $z = F_i(x, y)$. Then $|\mathbf{n}_0 \cdot \mathbf{N}| = \cos\gamma \geq 0$, where γ is the angle between $\mathbf{n}_0$ and $\mathbf{N}$, the unit exterior normal to the surface. But $dS = \frac{1}{\cos\gamma} dx\, dy$ (See for example L. Brand, *Advanced Calculus*, 1955, §164.) Thus

$$\int_{\partial\Omega_i} |\mathbf{n}_0 \cdot \mathbf{N}|\, dS = \int_{S_0} dx\, dy = A_0.$$

It follows from (7) that

$$I_3 = A_0(\pm p_1 \pm p_2). \tag{8}$$

Note that the parenthesized term in (8) is always a pressure *difference* since $\partial\Omega_1$ and $\partial\Omega_2$ lie on opposite sides of S_0. For example, if the orientations are chosen as in the figure, we see that

$$I_3 = A_0(p_2 - p_1).$$

The treatment of the body force term is straightforward, i.e.,

$$I_4 \equiv \int_\Omega \mathbf{f} \cdot \mathbf{n}_0\, dV = \mathbf{f}_0 \cdot \mathbf{n}_0 L_0 A_0. \tag{9}$$

Replacing the terms in (2), by their respective equivalent forms (4), (6), (8), and (9) and assuming the orientations of the figure, we obtain the scalar momentum balance for the control volume Ω,

$$L_0 \frac{dW_0}{dt} + \frac{W_2 W_{2,0}}{A_2 \rho_2} - \frac{W_1 W_{1,0}}{A_1 \rho_1} + A_0(p_2 - p_1) = \mathbf{f}_0 \cdot \mathbf{n}_0 L_0 A_0. \tag{10}$$

3 Remarks

1. Although equation (10) is exact, it is not suitable for computation. In particular it is necessary to relate the mass flow rates W_0, W_1, W_2, $W_{1,0}$, and $W_{2,0}$. In this connection let us observe that by definition

$$\begin{aligned} W_i &= |(\rho\mathbf{q})_i| A_i \cos\theta_i \\ W_{i,0} &= |(\rho\mathbf{q})_i| A_i \cos\theta_{i,0}, \quad i = 1, 2, \end{aligned}$$

where θ_i is the angle between $\mathbf{q}_i$ and $\mathbf{n}_i$ and $\theta_{i,0}$ is the angle between $\mathbf{q}_i$ and $\mathbf{n}_0$. Eliminating the quantity $|(\rho\mathbf{q})_i| A_i$ between these relationships and substituting the result for $W_{i,0}$ in (10) gives

$$L_0 \frac{dW_0}{dt} + \frac{W_2^2}{A_2 \rho_2} \frac{\cos\theta_{2,0}}{\cos\theta_2} - \frac{W_1^2}{A_1 \rho_1} \frac{\cos\theta_{1,0}}{\cos\theta_1} + A_0(p_2 - p_1) = \mathbf{f}_0 \cdot \mathbf{n}_0 L_0 A_0. \tag{11}$$

Note that in the case where $\mathbf{n}_0 = \mathbf{n}_1 = \mathbf{n}_2$ (e.g., Ω is a straight length of pipe) the ratio of cosines in (11) is unity and it reduces to the usual "one dimensional" momentum balance

$$L_0 \frac{dW_0}{dt} + \frac{W_2^2}{A_2\rho_2} - \frac{W_1^2}{A_1\rho_1} + A_0(p_2 - p_1) = \mathbf{f}_0 \cdot \mathbf{n}_0 L_0 A_0.$$

More generally, if we *assume* that $\mathbf{q}_i$ is in the direction of $\mathbf{n}_i$, $i = 1, 2$ (i.e., the fluid velocity on S_i is essentially the normal velocity), then in place of (11) we obtain the approximate balance equation

$$L_0 \frac{dW_0}{dt} + \frac{W_2^2}{A_2\rho_2} \cos\theta_{2,0} - \frac{W_1^2}{A_1\rho_1} \cos\theta_{1,0} + A_0(p_2 - p_1) = \mathbf{f}_0 \cdot \mathbf{n}_0 L_0 A_0, \tag{12}$$

where now $\theta_{i,0}$ is the *known* angle between $\mathbf{n}_i$ and $\mathbf{n}_0$.

In many computer codes utilizing the above approach, "momentum" control volumes such as Ω are supplemented with a second set of interlaced "continuity" control volumes over which mass is conserved. The continuity control volumes typically have as part of their surfaces the *interior* cross sections of the momentum control volumes (e.g., S_0). This allows the mass flow rates W_1 and W_2 appearing in (12) to be expressed (say by averaging or interpolation) in terms of W_0 and the analogous flow rates of the momentum control volumes contiguous to Ω. With this understanding, the basic flow variables of the macroscopic system are then W_0 and its analogs.

2. A"macroscopic momentum balance" equation has been given by Bird, Stuart and Lightfoot in their text *Transport Phenomena.* (Equation (7.2-1) in the 1960 edition of the book.) We have not utilized this equation in the above development for two reasons:

   (a) Equation (7.2-1) is a vector equation and so requires further modification before a suitable scalar momentum balance can be obtained.

   (b) The term accounting for the pressure effects in (7.2-1) does not appear to be correct. Indeed, it has the form

   $$p_1\mathbf{S}_1 - p_2\mathbf{S}_2, \tag{13}$$

   where according to Bird, Stewart and Lightfoot, $\mathbf{S}_1$ and $\mathbf{S}_2$ are vectors "with magnitudes S_1 and S_2 respectively [A_1 and A_2 in our notation], and *with the direction of the prevailing time-smoothed velocity at sections 1 and 2."* (italics added) That is, the force due to pressure is treated as a convected quantity

in the same manner as mass or momentum. However, it is well known that pressure is a scalar potential whose fundamental defining property is that on any infinitesimal plane in the fluid the force that it engenders acts along the *normal* to that plane. (See for example, L. M. Milne-Thomson, *Theoretical Hydrodynamics*, Macmillan, 1955, pg. 7.) Since the sections 1 and 2 are planes within the fluid, the directions associated with the vectors $\mathbf{S}_1$ and $\mathbf{S}_2$ in (13) should not be those of fluid velocity vectors. This conclusion is also supported by the following reasoning. The pressure gradient in the Euler equations can be written as the divergence of pI where I is the identity tensor. Therefore, (in our notation)

$$\int_\Omega \nabla p \, dV = \int_\Omega \nabla \cdot pI \, dV = \int_{\partial\Omega} p\mathbf{N} \, dV,$$

and from the last integral we see that the relevant direction for the boundary pressure is along the normal to $\partial\Omega$. This suggests that the directions of $\mathbf{S}_1$ and $\mathbf{S}_2$ should more properly be those of the respective normals to sections 1 and 2, but even this choice does not resolve the problem of how to treat the surface integral over the remaining part of $\partial\Omega$.